

Loading of relativistic Maxwellian-type distributions revisited

Takayuki Umeda

Information Initiative Center, Hokkaido University, Sapporo City, Hokkaido 060-0811, JAPAN

Abstract

A simple numerical method for loading of a relativistic Maxwellian-type distribution is proposed based on inverse transform sampling. The relativistic Maxwellian energy distribution is introduced as an alternative to the Maxwell-Jüttner distribution. The cumulative distribution of the shifted-Maxwellian energy distribution is approximated by an invertible function. Random variates of energy is transformed from uniformly distributed random variables. Then, the energy variates are converted to momentum vector variates. Numerical tests are presented to show that the present method successfully reproduce the relativistic Maxwellian energy distribution.

Keywords: Distribution function; Relativistic Maxwellian distribution; Random number generation; Inverse transform sampling

1. Introduction

Numerical techniques for loading of random variates from a certain distribution play an important role for initializing particle velocities in particle

Email address: umeda@iic.hokudai.ac.jp (Takayuki Umeda)

kinetic simulations such as Monte Carlo and particle-in-cell (PIC) simulations. There are two methods to generate random variates from a target distribution by utilizing random variables from a proposal (source) distribution. One is rejection sampling, which accepts a variable from a proposal distribution as a variate if a certain condition due to the target distribution is true, otherwise rejects it if false. Rejection sampling is inefficient (i.e., the acceptance rate is low) if the choice of a proposal distribution is not good. Hence, rejection sampling is sometimes unsuitable for high-performance computing.

Alternatively, inverse transform sampling converts random variables from a uniform distribution into variates from a target distribution by utilizing the inverse cumulative distribution function of the target distribution. However, there are many target distributions that are not integrable analytically. There are also many cumulative distributions that are not invertible analytically.

For non-relativistic particles, the Maxwell-Boltzmann or Maxwellian velocity distribution is commonly used as an initial velocity distribution. There is a classic inverse transform method for the Maxwellian distribution in two dimensions, which is well known as the Box-Muller transform [1]. It is easy to extend the Box-Muller transform for isotropic Maxwellian velocity distributions to anisotropic and/or drifting (shifted) non-relativistic velocity distributions.

For relativistic particles, the Maxwell-Jüttner distribution [2] is commonly used as an initial momentum distribution. Because of its difficulty and importance in numerical simulations, a numerical method for generating random variates from the Maxwell-Jüttner distribution is an issue for a half

century (see Ref. [3] and references therein). Rejection sampling is widely used for the Maxwell-Jüttner distribution [4, 5, 7, 6, 8, 3, 9]. To use inverse transform sampling, a numerical table for the cumulative distribution of the Maxwell-Jüttner distribution is necessary [10], because it is difficult to obtain an analytic expression for the cumulative distribution. However, the resolution of the table and the procedure of numerical interpolation affect the accuracy of the inverse cumulative distribution.

In the present study, a simple numerical method for loading of a relativistic and shifted Maxwellian-type distribution is proposed based on inverse transform sampling. In Sec. 2, the relativistic Maxwellian energy distribution is introduced as an alternative to the Maxwell-Jüttner distribution. Then a numerical method for loading of the relativistic shifted-Maxwellian energy distribution is presented. In Sec. 3, a comparison is made between the relativistic Maxwellian energy distribution and the Maxwell-Jüttner distribution. Properties (mean velocity, mean momentum, thermal energy and kinetic energy) of the two distributions are also given. Finally in Sec. 4, the summary of the present study is presented.

2. Maxwellian Energy Distribution

2.1. Non-relativistic and isotropic Maxwellian

The non-relativistic and isotropic Maxwellian velocity distribution is given as

$$f(\mathbf{v}) = \left(\sqrt{\frac{m}{2\pi T}} \right)^3 \exp\left(-\frac{m|\mathbf{v}|^2}{2T} \right), \quad (1)$$

where

$$\int_{-\infty}^{\infty} \int_{-\infty}^{\infty} \int_{-\infty}^{\infty} f(\mathbf{v}) d^3\mathbf{v} = 1.$$

For an isotropic velocity distribution, the velocity vector \mathbf{v} in Cartesian coordinates is converted to spherical coordinates as follows,

$$d^3\mathbf{v} = v^2 \sin\theta dv d\theta d\phi = 4\pi v^2 dv.$$

Then, equation (1) is written in terms of the scalar velocity $v \equiv |\mathbf{v}|$ as

$$f_v(v) = \sqrt{\frac{2}{\pi}} \left(\sqrt{\frac{m}{T}} \right)^3 v^2 \exp\left(-\frac{mv^2}{2T}\right), \quad (2)$$

where

$$\int_0^\infty f_v(v) dv = 1.$$

Wolfram Mathematica [11] is used for confirmation of this integral.

Alternatively, equation (2) is also rewritten in terms of the kinetic energy $\mathcal{K} \equiv mv^2/2$ as [12]

$$f_{\mathcal{K}}(\mathcal{K}) = \frac{2}{\sqrt{\pi}T} \sqrt{\frac{\mathcal{K}}{T}} \exp\left(-\frac{\mathcal{K}}{T}\right), \quad (3)$$

where

$$\int_0^\infty f_{\mathcal{K}}(\mathcal{K}) d\mathcal{K} = 1.$$

This integral is confirmed with Mathematica. Note that the following property is used,

$$d\mathcal{K} = mv dv, \quad \sqrt{\frac{2\mathcal{K}}{m^3}} d\mathcal{K} = v^2 dv.$$

Equation (3) is known as the Maxwellian “energy” distribution.

2.2. Relativistic and isotropic Maxwellian

The relativistic and isotropic Maxwellian energy distribution is given by replacing \mathcal{K} in Eq. (3) with $mc^2(\gamma - 1)$ as

$$f_\gamma(\gamma) = \frac{2}{\sqrt{\pi}} \frac{mc^2}{T} \sqrt{\frac{mc^2}{T}(\gamma - 1)} \exp\left\{-\frac{mc^2}{T}(\gamma - 1)\right\} \quad (4)$$

with γ being the relativistic Lorentz factor, where

$$\int_1^\infty f_\gamma(\gamma) d\gamma = 1.$$

The thermal energy is given by performing the following integral,

$$\int_1^\infty mc^2(\gamma - 1)f_\gamma(\gamma) d\gamma = \frac{3}{2}T. \quad (5)$$

These integrals are confirmed with Mathematica.

Equation (4) is written in terms of the scalar momentum $u \equiv \gamma v$ as

$$f_u(u) = \frac{2}{\sqrt{\pi}} \left(\sqrt{\frac{m}{T}} \right)^3 \frac{u^2}{\sqrt{1 + \frac{u^2}{c^2}} \sqrt{\sqrt{1 + \frac{u^2}{c^2}} + 1}} \exp \left\{ -\frac{mc^2}{T} \left(\sqrt{1 + \frac{u^2}{c^2}} - 1 \right) \right\}, \quad (6)$$

where

$$\int_0^\infty f_u(u) du = 1.$$

This integral is confirmed with Mathematica. Note that the following property is used,

$$\gamma = \sqrt{1 + \frac{u^2}{c^2}}, \quad c^2 \gamma d\gamma = u du.$$

Alternatively, equation (4) is also rewritten in terms of the momentum vector \mathbf{u} as

$$f(\mathbf{u}) = \frac{1}{2} \left(\sqrt{\frac{m}{\pi T}} \right)^3 \frac{1}{\gamma(\mathbf{u}) \sqrt{\gamma(\mathbf{u}) + 1}} \exp \left[-\frac{mc^2}{T} \{ \gamma(\mathbf{u}) - 1 \} \right], \quad (7)$$

where

$$\int_{-\infty}^\infty \int_{-\infty}^\infty \int_{-\infty}^\infty f(\mathbf{u}) d^3\mathbf{u} = 1.$$

This integral is confirmed by using a numerical integration. Note that the following property is used,

$$d^3\mathbf{u} = u^2 \sin \theta du d\theta d\phi = c^3 \gamma \sqrt{\gamma^2 - 1} \sin \theta d\gamma d\theta d\phi \quad (8)$$

with

$$\int_0^\pi \sin \theta d\theta = 2, \quad \int_0^{2\pi} d\phi = 2\pi.$$

2.3. Relativistic shifted-Maxwellian

A relativistic shifted-Maxwellian energy distribution in terms of the momentum vector is given by replacing γ in Eq. (7) with the boosted Lorentz factor γ_B and performing renormalization as

$$f(\mathbf{u}) = \frac{1}{2\gamma_D} \left(\sqrt{\frac{m}{\pi\gamma_D T}} \right)^3 \frac{1}{\gamma_B(\mathbf{u}) \sqrt{\gamma_B(\mathbf{u}) + 1}} \exp \left[-\frac{mc^2}{\gamma_D T} \{ \gamma_B(\mathbf{u}) - 1 \} \right], \quad (9)$$

where

$$\gamma_B = \gamma_D \left(\gamma - \frac{\mathbf{v}_D \cdot \mathbf{u}}{c^2} \right) \quad (10)$$

with the drift velocity vector \mathbf{v}_D and its Lorentz factor

$$\gamma_D = \frac{c^2}{\sqrt{c^2 - |\mathbf{v}_D|^2}}. \quad (11)$$

The following integral is confirmed by using a numerical integration,

$$\int_{-\infty}^{\infty} \int_{-\infty}^{\infty} \int_{-\infty}^{\infty} f(\mathbf{u}) d^3\mathbf{u} = 1.$$

The transformation from the Lorentz-factor-spherical coordinate to the momentum-vector-Cartesian coordinate is performed with following properties,

$$u_x = \gamma_D \left(c\sqrt{\gamma_B^2 - 1} \cos \theta + \gamma_B v_D \right), \quad (12a)$$

$$u_y = c\sqrt{\gamma_B^2 - 1} \sin \theta \cos \phi, \quad (12b)$$

$$u_z = c\sqrt{\gamma_B^2 - 1} \sin \theta \sin \phi. \quad (12c)$$

Here, the momentum vector coordinate is taken so that the u_x axis is parallel to the drift velocity vector \mathbf{v}_D . Then, the following property is obtained by using the Jacobian determinant (see Appendix A for details),

$$d^3\mathbf{u} = c^2\gamma_D \left(c\gamma_B + v_D\sqrt{\gamma_B^2 - 1} \cos\theta \right) \sqrt{\gamma_B^2 - 1} \sin\theta d\gamma_B d\theta d\phi. \quad (13)$$

Hence, the relativistic shifted-Maxwellian energy distribution in terms of the boosted Lorentz factor and the polar angle is given as follows,

$$f_{\gamma_B, \theta}(\gamma_B, \theta) = \frac{1}{\sqrt{\pi}} \left(\sqrt{\frac{mc^2}{\gamma_D T}} \right)^3 \left(1 + \frac{v_D}{c\gamma_B} \sqrt{\gamma_B^2 - 1} \cos\theta \right) \sqrt{\gamma_B - 1} \sin\theta \exp \left\{ -\frac{mc^2}{\gamma_D T} (\gamma_B - 1) \right\}, \quad (14)$$

where

$$\int_1^\infty \int_0^\pi f_{\gamma_B, \theta}(\gamma_B, \theta) d\theta d\gamma_B = 1.$$

This integral is confirmed by using Mathematica. By integrating Eq. (14) over θ , the following distribution in terms of the boosted Lorentz factor is obtained, which is identical to Eq. (4),

$$f_{\gamma_B}(\gamma_B) = \int_0^\pi f_{\gamma_B, \theta}(\gamma_B, \theta) d\theta = \frac{2}{\sqrt{\pi}} \left(\sqrt{\frac{mc^2}{\gamma_D T}} \right)^3 \sqrt{\gamma_B - 1} \exp \left\{ -\frac{mc^2}{\gamma_D T} (\gamma_B - 1) \right\}. \quad (15)$$

2.4. Inverse transform sampling

With the normalized (dimensionless) energy $\mathcal{E} = \frac{mc^2}{\gamma_D T}(\gamma_B - 1)$, equation (15) is rewritten as

$$f_{\mathcal{E}}(\mathcal{E}) = \frac{2}{\sqrt{\pi}} \sqrt{\mathcal{E}} \exp \{-\mathcal{E}\}, \quad (16)$$

where

$$\int_0^\infty f_{\mathcal{E}}(\mathcal{E}) d\mathcal{E} = 1.$$

This integral is confirmed with Mathematica. The cumulative distribution of Eq. (16) is given as

$$F_{\mathcal{E}}(x) = \int_0^x f_{\mathcal{E}}(\mathcal{E}) d\mathcal{E} = 1 - \frac{2}{\sqrt{\pi}} \Gamma\left(\frac{3}{2}, x\right) = \operatorname{erf}(\sqrt{x}) - \frac{2}{\sqrt{\pi}} \sqrt{x} e^{-x}. \quad (17)$$

This integral is confirmed with Mathematica. Here, $\Gamma(n, x)$ is the upper incomplete Gamma function,

$$\Gamma\left(\frac{3}{2}, x\right) = \frac{1}{2} \Gamma\left(\frac{1}{2}, x\right) + \sqrt{x} e^{-x} = \frac{\sqrt{\pi}}{2} \{1 - \operatorname{erf}(\sqrt{x})\} + \sqrt{x} e^{-x}.$$

Since there is no analytic inverse function of the cumulative distribution in Eq. (17), the following approximation is utilized [13, 14],

$$F_{\mathcal{E}}(x) \approx \left\{ 1 - \exp\left(-\frac{ax + bx^2}{1 + cx + dx^2}\right) \right\}^{\frac{3}{2}} \equiv F_{\text{app}}(x). \quad (18)$$

It is noted that the coefficients a , b , c and d must be constant to make Eq. (18) invertible. The Taylor series expansion of Eqs. (17) and (18) around $x = 0$ are derived with Mathematica as follows,

$$F_{\mathcal{E}}(x) \approx \frac{4}{3\sqrt{\pi}} x^{\frac{3}{2}} + O\left(x^{\frac{5}{2}}\right),$$

$$F_{\text{app}}(x) \approx (ax)^{\frac{3}{2}} + O\left(x^{\frac{5}{2}}\right).$$

Hence, the coefficient a is obtained as

$$a = \left(\frac{16}{9\pi}\right)^{\frac{1}{3}}.$$

To obtain the other coefficients b , c and d , a brute-force search is performed to minimize the root mean square of numerical errors between Eqs. (17) and (18) for $0 < x \leq 8$, which gives $b = -3.12562 \times 10^{-2}$, $c = -5.15921 \times 10^{-2}$ and $d = 8.84448 \times 10^{-4}$.

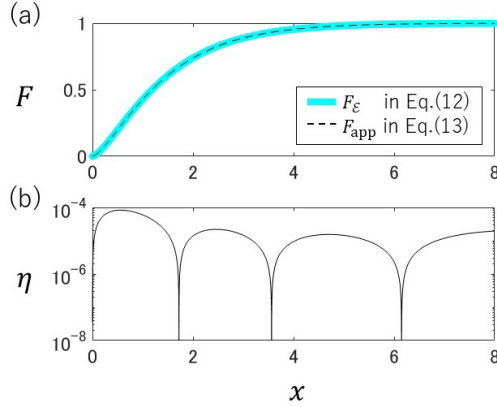


Figure 1: Comparison between the cumulative distribution $F_{\mathcal{E}}$ in Eq. (17) and its approximation F_{app} in Eq. (18). (a) The profiles of $F_{\mathcal{E}}$ and F_{app} for $0 < x \leq 8$. The thick line shows $F_{\mathcal{E}}$ and the dashed line shows F_{app} . (b) The relative error η between $F_{\mathcal{E}}$ and F_{app} .

Figure 1 shows the comparison between the cumulative distribution in Eq. (17) and its approximation in Eq. (18) with the coefficients listed above. In Panel (a), spatial profiles of these functions are shown. In Panel (b), the relative error between Eqs. (17) and (18), i.e., $\eta = |(F_{\mathcal{E}} - F_{\text{app}})/F_{\mathcal{E}}|$, is shown. It is found that the relative error of the approximated cumulative distribution is less than 10^{-4} .

The inverse function of Eq. (18) is given as

$$\mathcal{Y} = \log \left(1 - y^{\frac{2}{3}} + \varepsilon \right),$$

$$F_{\text{app}}^{-1}(y) = \frac{\sqrt{\{a + c\mathcal{Y}(y)\}^2 - 4\mathcal{Y}(y)\{b + d\mathcal{Y}(y)\}} - \{a + c\mathcal{Y}(y)\}}{2\{b + d\mathcal{Y}(y)\}}, \quad (19)$$

for $0 \leq x < 1$. Here, ε denotes a small variable (e.g., 2^{-126}) to avoid taking zero as an argument of the logarithm function.

Random variates from Maxwellian energy distribution are generated with

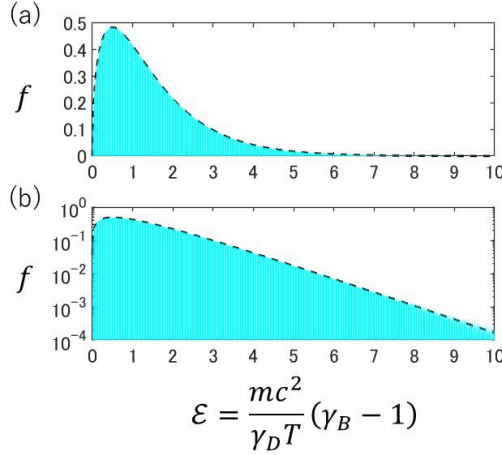


Figure 2: Comparison between the Maxwellian energy distribution in Eq. (16) and a histogram of numerically generated random variates. The dashed lines show the profile of Eq. (16) as a function of the normalized energy $\mathcal{E} = mc^2(\gamma_B - 1)/(\gamma_D T)$ in (a) a linear scale and (b) a logarithmic scale. The bars show a histogram of random variates generated by using Eq. (20) with $N_s = 10^8$ samples and $N_{\text{bin}} = 10^4$ bins.

random variables from uniform distribution, $0 \leq R_n^{(1)} < 1$, as follows,

$$\mathcal{E}_n = F_{\text{app}}^{-1} (R_n^{(1)} R_{\text{ul}}). \quad (20)$$

where R_{ul} denotes the upper limit for the argument of the inverse function in Eq. (19), which is introduced to avoid taking a negative number as an operand of square root in Eq. (19). With the coefficients listed above, the upper limit is given as $R_{\text{ul}} \approx 0.999997546$.

Figure 2 shows the comparison between the Maxwellian energy distribution in Eq. (16) and a histogram of numerically generated random variates. The dashed lines show the profile of Eq. (16) as a function of the normalized energy $\mathcal{E} = mc^2(\gamma_B - 1)/(\gamma_D T)$ in (a) a linear scale and (b) a logarithmic scale. The bars show a histogram of random variates generated by using Eq.

(20). The histogram is created with $N_s = 10^8$ samples and $N_{\text{bin}} = 10^4$ bins. The result shows an excellent agreement between the analytic distribution and the histogram.

In general, variates for energy (or scalar momentum) in spherical coordinates are converted to variates for momentum vector with other two sets of random variables from uniform distribution, $0 \leq R_n^{(2)} < 1$ and $0 \leq R_n^{(3)} < 1$, via

$$\theta_n = \cos^{-1} (2R_n^{(2)} - 1), \quad (21a)$$

$$\phi_n = 2\pi R_n^{(3)}. \quad (21b)$$

Equation (21a) is rewritten as the following well-known identities,

$$\cos \theta_n = \cos [\cos^{-1} (2R_n^{(2)} - 1)] = 2R_n^{(2)} - 1,$$

$$\sin \theta_n = \sin [\cos^{-1} (2R_n^{(2)} - 1)] = \sqrt{1 - (2R_n^{(2)} - 1)^2} = 2\sqrt{R_n^{(2)} (1 - R_n^{(2)})}.$$

For a general relativistic distribution, however, it is not able to transform from the boosted-Lorentz-factor coordinate (i.e., f_{γ_B}) to the momentum-vector coordinate (i.e., f) by using Eq. (21). As shown below, the distribution obtained by the coordinate transformation with Eq. (21) is not an equilibrium distribution (i.e., a function of γ_B) unlike Eq. (9) (see Appendix A for details),

$$f(\mathbf{u}) = \frac{4\pi}{\gamma(\mathbf{u}) \sqrt{\gamma_B^2(\mathbf{u}) - 1}} f_{\gamma_B} \{ \gamma_B(\mathbf{u}) \}.$$

A general relativistic distribution in terms of the momentum vector (f) is converted to a relativistic distribution in terms of both boosted Lorentz factor and polar angle ($f_{\gamma_B, \theta}$) with Eq. (13) as follows,

$$f_{\gamma_B, \theta}(\gamma_B, \theta) = \frac{c^2}{4\pi} \sqrt{\gamma_B^2 - 1} \sin \theta \left(c\gamma_B + v_D \sqrt{\gamma_B^2 - 1} \cos \theta \right) f(\mathbf{u}).$$

Since the relativistic distribution is expressed as a function of the polar angle as well as the boosted Lorentz factor, it is necessary to take the $v_D (\neq 0)$ term into account, which is excluded in Eq. (21a). The normalized cumulative distribution of Eq. (14) in terms of the polar angle is given as

$$F_{\gamma_B, \theta}(x) = \frac{1}{2} (1 - \cos x) + \frac{v_D}{2c} \sqrt{1 - \frac{1}{\gamma_B^2}} (1 - \cos^2 x). \quad (22)$$

The inverse function of this cumulative distribution is given as

$$F_{\gamma_B, \theta}^{-1}(y) = \cos^{-1} \left[\frac{\sqrt{1 + \frac{v_D^2}{c^2} \left(1 - \frac{1}{\gamma_B^2}\right) + \frac{2v_D}{c} \sqrt{1 - \frac{1}{\gamma_B^2}} (1 - 2y)} - 1}{\frac{v_D}{c} \sqrt{1 - \frac{1}{\gamma_B^2}}} \right]. \quad (23)$$

To summarize, three sets of random variables from uniform distribution, $R_n^{(1)}$, $R_n^{(2)}$ and $R_n^{(3)}$, are converted to variates of boosted Lorentz factor, polar angle, and azimuth angle as follows,

$$\gamma_{B,n} = 1 + \frac{\gamma_D T}{mc^2} F_{\text{app}}^{-1}(R_n^{(1)} R_{\text{ul}}), \quad (24a)$$

$$\theta_n = \begin{cases} F_{\gamma_B, \theta}^{-1}(R_n^{(2)}) & (v_D \neq 0), \\ \cos^{-1}(2R_n^{(2)} - 1) & (v_D = 0), \end{cases} \quad (24b)$$

$$\phi_n = 2\pi R_n^{(3)}, \quad (24c)$$

by using the inverse functions in Eqs. (19) and (23). Then, these variates are transformed into variates of momentum vector by using Eq. (12). With these procedures, the relativistic shifted-Maxwellian energy distribution in terms of the momentum vector in Eq. (9) is obtained.

With the following property [16],

$$d^3\mathbf{u} = \gamma^5 d^3\mathbf{v},$$

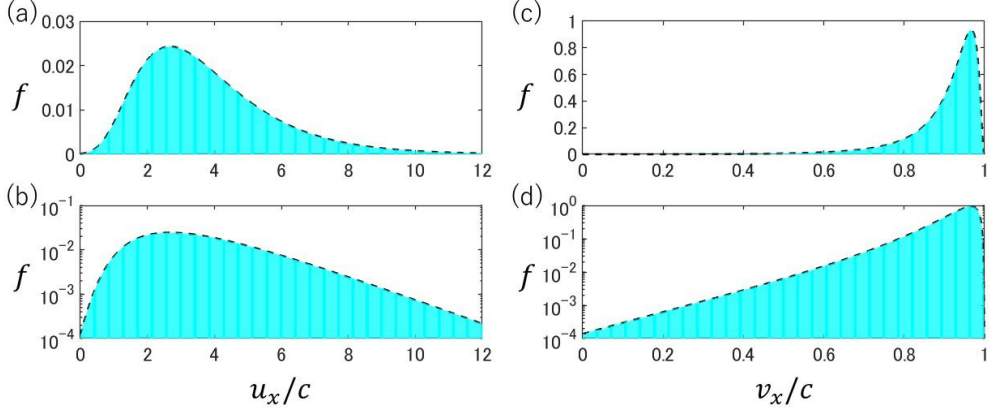


Figure 3: Comparison between the momentum/velocity distribution based on the Maxwellian energy distribution and a histogram of numerically generated random variates. The dashed lines in the left panels show the reduced momentum distribution in the u_x direction with $v_D/c = 0.9$ and $mc^2/T = 6.25$ in (a) a linear scale and (b) a logarithmic scale. The dashed lines in the right panels show the corresponding reduced velocity distribution in the v_x direction in (c) a linear scale and (d) a logarithmic scale. The bars show a histogram of random variates generated by using Eqs. (12) and (24) with $N_s = 10^8$ samples and $N_{\text{bin}} = 10^4$ bins.

the momentum distribution in Eq. (9) is rewritten in terms of the velocity vector as follows,

$$f_v(\mathbf{v}) = \frac{1}{2\gamma_D} \left(\sqrt{\frac{m}{\pi\gamma_D T}} \right)^3 \frac{\gamma^5(\mathbf{v})}{\gamma_B(\mathbf{v}) \sqrt{\gamma_B(\mathbf{v}) + 1}} \exp \left[-\frac{mc^2}{\gamma_D T} \{\gamma_B(\mathbf{v}) - 1\} \right], \quad (25)$$

where

$$\int_{-\infty}^{\infty} \int_{-\infty}^{\infty} \int_{-\infty}^{\infty} f(\mathbf{v}) d^3\mathbf{v} = 1.$$

This integral is confirmed by using a numerical integration.

Figure 3 shows the comparison between the momentum/velocity distribution and a histogram of numerically generated random variates. The dashed

lines in the left panels show the reduced momentum distribution in terms of u_x with $v_D/c = 0.9$ and $mc^2/T = 6.25$. The dashed lines in the right panels show the corresponding reduced velocity distribution in terms of v_x . Since it is not easy to analytically integrate the distributions in Eqs. (9) and (25) over the $u_y - u_z$ space and the $v_y - v_z$ space (i.e., the momentum/velocity space perpendicular to the drift velocity vector) respectively, a numerical integration is performed to obtain the reduced momentum and velocity distributions in the u_x and v_x directions. The bars show a histogram of random variates generated by using Eqs. (12) and (24). The histogram is created with $N_s = 10^8$ samples and $N_{\text{bin}} = 10^4$ bins. The result shows an excellent agreement between the analytic distribution and the histogram.

3. Comparison against Maxwell-Jüttner Distribution

The Maxwell-Jüttner distribution in terms of the momentum vector \mathbf{u} is given as

$$g(\mathbf{u}) = \frac{m}{4\pi cTK_2\left(\frac{mc^2}{T}\right)} \exp\left(-\frac{mc^2}{T} \sqrt{1 + \frac{|\mathbf{u}|^2}{c^2}}\right), \quad (26)$$

where K_n denotes the modified Bessel function of the second kind of order n . For an isotropic distribution, this distribution is alternatively written by utilizing Eq. (8) in terms of the scalar momentum u as

$$g_u(u) = \frac{mu^2}{cTK_2\left(\frac{mc^2}{T}\right)} \exp\left(-\frac{mc^2}{T} \sqrt{1 + \frac{u^2}{c^2}}\right), \quad (27)$$

or in terms of the Lorentz factor γ as

$$g_\gamma(\gamma) = \frac{mc^2}{T} \frac{\gamma\sqrt{\gamma^2 - 1}}{K_2\left(\frac{mc^2}{T}\right)} \exp\left(-\frac{mc^2}{T} \gamma\right), \quad (28)$$

where

$$\int_1^{\infty} g_{\gamma}(\gamma) d\gamma = 1.$$

This integral is confirmed with Mathematica.

Similarly to Eq. (9), the shifted Maxwell-Jüttner distribution in terms of the momentum vector is given with the boosted Lorentz factor γ_B as [16]

$$g(\mathbf{u}) = \frac{m}{4\pi c\gamma_D T K_2\left(\frac{mc^2}{T}\right)} \exp\left\{-\frac{mc^2}{T}\gamma_B(\mathbf{u})\right\}. \quad (29)$$

This is rewritten in terms of the boosted Lorentz factor as follows,

$$g_{\gamma_B}(\gamma_B) = \frac{mc^2}{TK_2\left(\frac{mc^2}{T}\right)} \gamma_B \sqrt{\gamma_B^2 - 1} \exp\left(-\frac{mc^2}{T}\gamma_B\right). \quad (30)$$

With the normalized energy $\mathcal{E}' = mc^2(\gamma_B - 1)/T$, equation (30) is rewritten as

$$g_{\mathcal{E}}(\mathcal{E}', T) = \frac{T^2}{m^2 c^4 K_2\left(\frac{mc^2}{T}\right)} \sqrt{\mathcal{E}'\left(\mathcal{E}' + 2\frac{mc^2}{T}\right)} \left(\mathcal{E}' + \frac{mc^2}{T}\right) \exp\left\{-\left(\mathcal{E}' + \frac{mc^2}{T}\right)\right\}, \quad (31)$$

where

$$\int_0^{\infty} g_{\mathcal{E}}(\mathcal{E}') d\mathcal{E}' = 1.$$

This integral is confirmed with Mathematica. There is no analytic expression of the cumulative distribution of Eq. (31).

Figure 4 shows the comparison between the relativistic Maxwellian energy distribution in Eq. (16) and the Maxwell-Jüttner distribution in Eq. (31) as a function of the normalized energy \mathcal{E}' . The solid line shows the profile of Eq. (16) with $\gamma_D = 1$. The circles show the profile of Eq. (31) with $mc^2/T = 100$. The squares show the profile of Eq. (31) with $mc^2/T = 1$. The triangles show the profile of Eq. (31) with $mc^2/T = 0.01$. With a smaller

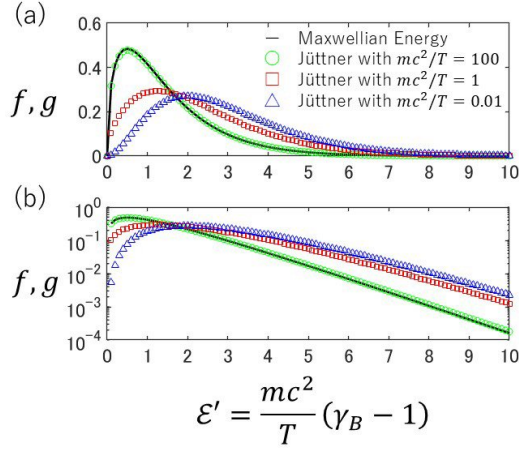


Figure 4: Comparison between the Maxwellian energy distribution in Eq. (16) and the Maxwell-Jüttner distribution in Eq. (31) with different mc^2/T in (a) a linear scale and (b) a logarithmic scale. The solid line shows the profile of Eq. (16) with $\gamma_D = 1$. The circles show the profile of Eq. (31) with $mc^2/T = 100$. The squares show the profile of Eq. (31) with $mc^2/T = 1$. The triangles show the profile of Eq. (31) with $mc^2/T = 0.01$.

T , the Maxwell-Jüttner distribution approaches to the Maxwellian energy distribution. However, the high-energy tail of the Maxwell-Jüttner distribution is more enhanced with a larger T . The Maxwell-Jüttner distribution is expressed as a function of both \mathcal{E}' and T . It is not easy to approximate the cumulative distribution of Eq. (31) by using an invertible function such as Eq. (18), because the coefficients are given as a function of T .

Alternatively, rejection sampling was applied to the reduced Maxwell-Jüttner distribution [7, 9], in which the Maxwell-Jüttner distribution in Eq. (29) is transforming to cylindrical coordinates and analytically integrated

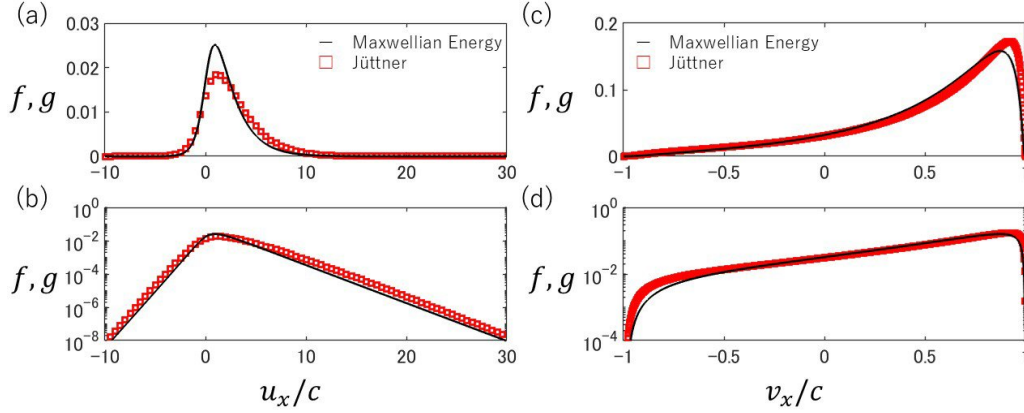


Figure 5: Comparison between the relativistic Maxwellian energy distribution in Eq. (9) and the Maxwell-Jüttner distribution in Eq. (29) with $v_D/c = 0.5$ and $mc^2/T = 1$. Left panels show the reduced momentum distribution in the u_x space in (a) a linear scale and (b) a logarithmic scale. Right panels show the reduced velocity distribution in the v_x space in (c) a linear scale and (d) a logarithmic scale. The solid line shows the profile of the reduced Maxwellian energy distribution. The squares show the profile of the reduced Maxwell-Jüttner distribution.

over the perpendicular momentum space as follows [7, 10],

$$g_{u_x}(u_x) = \frac{T}{2mc^3\gamma_D^3 K_2\left(\frac{mc^2}{T}\right)} \left(1 + \frac{mc^2\gamma_D}{T} \sqrt{1 + \frac{u_x^2}{c^2}}\right) \exp\left\{-\frac{mc^2\gamma_D}{T} \left(\sqrt{1 + \frac{u_x^2}{c^2}} - \frac{v_D u_x}{c^2}\right)\right\}. \quad (32)$$

This is reconfirmed by using Mathematica as well as a numerical integration.

Figure 5 shows the comparison between the relativistic Maxwellian energy distribution in Eq. (9) and the Maxwell-Jüttner distribution in Eq. (29) with $v_D/c = 0.5$ and $mc^2/T = 1$. Left panels show the reduced momentum distribution in the u_x space in (a) a linear scale and (b) a logarithmic scale. Right panels show the reduced velocity distribution in the v_x space in (c) a linear scale and (d) a logarithmic scale. The solid lines show the reduced

Maxwellian energy distribution as a function of the momentum u_x and the velocity v_x , which are obtained by using a numerical integration over the $u_y - u_z$ space and $v_y - v_z$ space, respectively. The squares show the reduced Maxwell-Jüttner distribution in Eq. (29) obtained by a numerical integration. Note that the reduced Maxwell-Jüttner distribution in the u_x space is given in Eq. (32) as well.

With a larger mc^2/T (i.e., smaller T), the Maxwell-Jüttner distribution approaches to the Maxwellian energy distribution. With a smaller mc^2/T (i.e., larger T), high-energy components are more enhanced in the Maxwell-Jüttner distribution, and the peak of the distribution shifts toward a high energy side.

In both velocity distributions, the mean velocity is given as follows,

$$\int_{-c}^c \int_{-c}^c \int_{-c}^c \mathbf{v} \gamma^5(\mathbf{v}) f \left(\frac{c\mathbf{v}}{\sqrt{c^2 - |\mathbf{v}|^2}} \right) d^3\mathbf{v} = \int_{-c}^c \int_{-c}^c \int_{-c}^c \mathbf{v} \gamma^5(\mathbf{v}) g \left(\frac{c\mathbf{v}}{\sqrt{c^2 - |\mathbf{v}|^2}} \right) d^3\mathbf{v} = \mathbf{v}_D, \quad (33)$$

which is confirmed by a numerical integration.

The mean momentum of the Maxwell-Jüttner distribution is given as follows [16],

$$\int_{-\infty}^{\infty} \int_{-\infty}^{\infty} \int_{-\infty}^{\infty} \mathbf{u} g(\mathbf{u}) d^3\mathbf{u} = \frac{K_3 \left(\frac{mc^2}{T} \right)}{K_2 \left(\frac{mc^2}{T} \right)} \gamma_D \mathbf{v}_D, \quad (34)$$

which is reconfirmed by a numerical integration. However, the mean momentum of the Maxwellian energy distribution is given as follows (see Appendix B for detail),

$$\int_{-\infty}^{\infty} \int_{-\infty}^{\infty} \int_{-\infty}^{\infty} \mathbf{u} f(\mathbf{u}) d^3\mathbf{u}$$

$$= \left(\frac{4}{3} + \frac{2\gamma_D T}{mc^2} - \frac{2mc^2}{3\gamma_D T} \left[1 - \sqrt{\frac{\pi mc^2}{\gamma_D T}} \exp\left(\frac{mc^2}{\gamma_D T}\right) \left\{ 1 - \operatorname{erf}\left(\sqrt{\frac{mc^2}{\gamma_D T}}\right) \right\} \right] \right) \gamma_D v_D, \quad (35)$$

which is slightly smaller than the mean momentum of the Maxwell-Jüttner distribution in Eq. (34).

A useful property is obtained by performing the following integral for the Maxwell-Jüttner distribution,

$$\int_{-\infty}^{\infty} \int_{-\infty}^{\infty} \int_{-\infty}^{\infty} mc^2 \{\gamma_B(\mathbf{u}) - 1\} g(\mathbf{u}) d^3\mathbf{u} = T \left[3 - \frac{mc^2}{T} \left\{ 1 - \frac{K_1\left(\frac{mc^2}{T}\right)}{K_2\left(\frac{mc^2}{T}\right)} \right\} \right]. \quad (36)$$

This integral is confirmed with Mathematica. This property is related to the thermal energy, which approaches to $3T/2$ with larger mc^2/T but is enhanced with smaller mc^2/T . The property related to the thermal energy for the Maxwellian energy distribution is given as follows,

$$\int_{-\infty}^{\infty} \int_{-\infty}^{\infty} \int_{-\infty}^{\infty} mc^2 \{\gamma_B(\mathbf{u}) - 1\} f(\mathbf{u}) d^3\mathbf{u} = \frac{3}{2} \gamma_D T. \quad (37)$$

The kinetic energy of the Maxwell-Jüttner distribution is obtained by performing the following integral,

$$\begin{aligned} & \int_{-\infty}^{\infty} \int_{-\infty}^{\infty} \int_{-\infty}^{\infty} mc^2 \{\gamma(\mathbf{u}) - 1\} g(\mathbf{u}) d^3\mathbf{u} \\ &= \frac{T}{\gamma_D} \left[3 - \frac{mc^2}{T} \left\{ 1 - \frac{K_1\left(\frac{mc^2}{T}\right)}{K_2\left(\frac{mc^2}{T}\right)} \right\} \right] + \left\{ \frac{K_3\left(\frac{mc^2}{T}\right)}{K_2\left(\frac{mc^2}{T}\right)} - \frac{1}{\gamma_D + 1} \right\} m\gamma_D v_D^2. \end{aligned} \quad (38)$$

This integral is confirmed with an numerical integration. The kinetic energy of the Maxwellian energy distribution is given as follows (see Appendix B for

detail),

$$\int_{-\infty}^{\infty} \int_{-\infty}^{\infty} \int_{-\infty}^{\infty} mc^2 \{\gamma_B(\mathbf{u}) - 1\} f(\mathbf{u}) d^3\mathbf{u} = \frac{3}{2}T + \left[\frac{4}{3} - \frac{1}{\gamma_D + 1} + \frac{2\gamma_D T}{mc^2} - \frac{2mc^2}{3\gamma_D T} \left\{ 1 - \sqrt{\frac{\pi mc^2}{\gamma_D T}} \exp\left(\frac{mc^2}{\gamma_D T}\right) \operatorname{erfc}\left(\sqrt{\frac{mc^2}{\gamma_D T}}\right) \right\} \right] m\gamma_D v_D^2. \quad (39)$$

This integral is confirmed with an numerical integration. The kinetic energy of the Maxwellian energy distribution is smaller than that of the Maxwell-Jüttner distribution in Eq. (38).

In both distributions, the bulk drift energy is given as follows,

$$\mathcal{D} = m\mathbf{v}_D \cdot \left(\langle \mathbf{u} \rangle - \frac{\gamma_D \mathbf{v}_D}{\gamma_D + 1} \right), \quad (40)$$

where $\langle \mathbf{u} \rangle$ denotes the mean momentum vector. Note that the mean velocity vector is given as $\langle \mathbf{v} \rangle = \mathbf{v}_D$ as described above. If $\langle \mathbf{u} \rangle = \gamma_D \mathbf{v}_D$, the bulk drift energy is expressed as $|\gamma_D \mathbf{v}_D|^2 / (\gamma_D + 1)$. In a non-relativistic limit (i.e., $\gamma_D \rightarrow 1$), the drift energy approaches to $m|\mathbf{v}_D|^2 / 2$.

It is able to separate the kinetic energy into the bulk drift energy and the thermal energy. The thermal energy of the Maxwellian energy distribution is given as $\mathcal{T} = 3T/2$. However, the thermal energy of the Maxwell-Jüttner distribution includes the enhancement due to mc^2/T and the decrease by a factor of γ_D due to the definition of the distribution.

4. Summary

Numerical methods for generating random variates from a relativistic Maxwellian-type distribution are important in relativistic particle kinetic simulations. Conventionally, rejection sampling is widely used to generate

random variates of momentum vector from the Maxwell-Jüttner distribution. Inverse transforms sampling has issues in integrability of a target distribution and invertibility of its cumulative distribution.

In the present study, a relativistic shifted-Maxwellian energy distribution is introduced as an alternative to the Maxwell-Jüttner distribution. To adopt the inverse transforms sampling, an invertible function is presented, which accurately approximate the cumulative distribution of the Maxwellian energy distribution. Then, random variates of momentum vector from the relativistic shifted-Maxwellian energy distribution are generated by utilizing three sets of random variables from uniform distribution. The numerical procedure of the present method is simple and easily implemented as an elemental function, i.e., $(u_x, u_y, u_z) = \text{func} \{R^{(1)}, R^{(2)}, R^{(3)}\}$, which is more suitable for high-performance computing.

Appendix A. Jacobian Determinant

From Eq. (12), the Jacobian matrix is given as

$$\mathbf{J} = \begin{bmatrix} \frac{\partial u_x}{\partial \gamma_B} & \frac{\partial u_x}{\partial \theta} & \frac{\partial u_x}{\partial \phi} \\ \frac{\partial u_y}{\partial \gamma_B} & \frac{\partial u_y}{\partial \theta} & \frac{\partial u_y}{\partial \phi} \\ \frac{\partial u_z}{\partial \gamma_B} & \frac{\partial u_z}{\partial \theta} & \frac{\partial u_z}{\partial \phi} \end{bmatrix}$$

$$= \begin{bmatrix} \gamma_D \left(\frac{c\gamma_B}{\sqrt{\gamma_B^2 - 1}} \cos \theta + v_D \right) & -c\gamma_D \sqrt{\gamma_B^2 - 1} \sin \theta & 0 \\ \frac{c\gamma_B}{\sqrt{\gamma_B^2 - 1}} \sin \theta \cos \phi & c\sqrt{\gamma_B^2 - 1} \cos \theta \cos \phi & -c\sqrt{\gamma_B^2 - 1} \sin \theta \sin \phi \\ \frac{c\gamma_B}{\sqrt{\gamma_B^2 - 1}} \sin \theta \sin \phi & c\sqrt{\gamma_B^2 - 1} \cos \theta \sin \phi & c\sqrt{\gamma_B^2 - 1} \sin \theta \cos \phi \end{bmatrix}. \quad (\text{A.1})$$

Then, the Jacobian determinant is given as

$$\det(\mathbf{J}) = c^3 \gamma_D \gamma_B \sqrt{\gamma_B^2 - 1} \sin \theta + c^2 v_D \gamma_D (\gamma_B^2 - 1) \cos \theta \sin \theta. \quad (\text{A.2})$$

This leads to Eq. (13).

From Eqs. (10) and (12a), equation (A.2) is rewritten as follows,

$$\begin{aligned} \det(\mathbf{J}) &= c^3 \gamma_D \sqrt{\gamma_B^2 - 1} \sin \theta \left(\gamma_B + \frac{v_D u_x}{c^2 \gamma_D} - \frac{\gamma_B v_D^2}{c^2} \right) = c^3 \sqrt{\gamma_B^2 - 1} \sin \theta \left(\frac{\gamma_B}{\gamma_D} + \frac{v_D u_x}{c^2} \right) \\ &= c^3 \gamma \sqrt{\gamma_B^2 - 1} \sin \theta. \end{aligned} \quad (\text{A.3})$$

Appendix B. Properties of Maxwellian Energy Distribution

Analytic expression of the mean momentum is obtained by using Eqs. (12a) and (14),

$$\begin{aligned} \int_{-\infty}^{\infty} \int_{-\infty}^{\infty} \int_{-\infty}^{\infty} u_x f(\mathbf{u}) d^3 \mathbf{u} &= \int_0^\pi \int_1^\infty \frac{1}{\sqrt{\pi}} \left(\sqrt{\frac{mc^2}{\gamma_D T}} \right)^3 \gamma_D \left(c \sqrt{\gamma_B^2 - 1} \cos \theta + \gamma_B v_D \right) \\ &\quad \left(1 + \frac{v_D}{c \gamma_B} \sqrt{\gamma_B^2 - 1} \cos \theta \right) \sqrt{\gamma_B - 1} \sin \theta \exp \left\{ -\frac{mc^2}{\gamma_D T} (\gamma_B - 1) \right\} d\gamma_B d\theta \\ &= \frac{2\gamma_D v_D}{\sqrt{\pi}} \left(\sqrt{\frac{mc^2}{\gamma_D T}} \right)^3 \int_1^\infty \left(\frac{1}{3} \frac{\gamma_B^2 - 1}{\gamma_B} + \gamma_B \right) \sqrt{\gamma_B - 1} \exp \left\{ -\frac{mc^2}{\gamma_D T} (\gamma_B - 1) \right\} d\gamma_B \\ &= \left[\frac{4}{3} + \frac{2\gamma_D T}{mc^2} - \frac{2mc^2}{3\gamma_D T} \left\{ 1 - \sqrt{\frac{\pi mc^2}{\gamma_D T}} \exp \left(\frac{mc^2}{\gamma_D T} \right) \operatorname{erfc} \left(\sqrt{\frac{mc^2}{\gamma_D T}} \right) \right\} \right] \gamma_D v_D, \end{aligned}$$

where $\operatorname{erfc}(x) = 1 - \operatorname{erf}(x)$ is the complementary error function. This is confirmed with Mathematica.

Analytic expression of the kinetic energy is obtained by using Eqs. (35) and (37),

$$\int_{-\infty}^{\infty} \int_{-\infty}^{\infty} \int_{-\infty}^{\infty} mc^2 \{ \gamma(\mathbf{u}) - 1 \} f(\mathbf{u}) d^3 \mathbf{u}$$

$$\begin{aligned}
&= \frac{1}{\gamma_D} \int_{-\infty}^{\infty} \int_{-\infty}^{\infty} \int_{-\infty}^{\infty} mc^2 \{\gamma_B(\mathbf{u}) - 1\} f(\mathbf{u}) d^3\mathbf{u} - mc^2 \\
&\quad + \frac{1}{\gamma_D} \int_{-\infty}^{\infty} \int_{-\infty}^{\infty} \int_{-\infty}^{\infty} mc^2 \left(\frac{v_D u_x}{c^2} + 1 \right) f(\mathbf{u}) d^3\mathbf{u} \\
&= \frac{3T}{2} + \frac{mc^2}{\gamma_D} (1 - \gamma_D) + \left[\frac{4}{3} + \frac{2\gamma_D T}{mc^2} - \frac{2mc^2}{3\gamma_D T} \left\{ 1 - \sqrt{\frac{\pi mc^2}{\gamma_D T}} \exp\left(\frac{mc^2}{\gamma_D T}\right) \operatorname{erfc}\left(\sqrt{\frac{mc^2}{\gamma_D T}}\right) \right\} \right] m\gamma_D v_D^2 \\
&= \frac{3T}{2} + \left[\frac{4}{3} - \frac{1}{\gamma_D + 1} + \frac{2\gamma_D T}{mc^2} - \frac{2mc^2}{3\gamma_D T} \left\{ 1 - \sqrt{\frac{\pi mc^2}{\gamma_D T}} \exp\left(\frac{mc^2}{\gamma_D T}\right) \operatorname{erfc}\left(\sqrt{\frac{mc^2}{\gamma_D T}}\right) \right\} \right] m\gamma_D v_D^2.
\end{aligned}$$

Appendix C. Loading of Anisotropic Distribution

Anisotropic Maxwell-Jüttner distributions are presented in Refs. [12, 15]. A shifted and anisotropic Maxwellian energy distribution is introduced as an extension of Ref. [15],

$$\gamma_A = \gamma_D \left(\sqrt{1 + \frac{T_{\perp}}{T_{\parallel}} \frac{u_x^2}{c^2} + \frac{u_y^2}{c^2} + \frac{u_z^2}{c^2} - \frac{v_D u_x}{c^2}} \right), \quad (\text{C.1a})$$

$$f(\mathbf{u}) = \frac{1}{2\gamma_D} \left(\sqrt{\frac{m}{\pi\gamma_D T_{\perp}}} \right)^3 \frac{1}{\gamma_A(\mathbf{u}) \sqrt{\gamma_A(\mathbf{u}) + 1}} \exp \left[-\frac{mc^2}{\gamma_D T_{\perp}} \{\gamma_A(\mathbf{u}) - 1\} \right]. \quad (\text{C.1b})$$

Here, the momentum vector coordinate is taken so that the u_x axis is parallel to the drift velocity vector \mathbf{v}_D , and T_{\parallel} and T_{\perp} are temperature components parallel and perpendicular to the drift velocity vector, respectively.

In addition to the following two conditions for $d\gamma_B/dt = 0$, $\mathbf{v}_D \cdot \mathbf{E} = 0$ and $\mathbf{E} \cdot \mathbf{B} = 0$, the third condition, $\mathbf{E} = 0$, is necessary to satisfy $d\gamma_A/dt = 0$. That is, the drift velocity vector must be parallel to the magnetic field, $\mathbf{v}_D \times \mathbf{B} = 0$ in relativistic shifted and anisotropic distributions.

Random of energy variates from Maxwellian energy distribution are generated by using Eq. (20). The energy variates are converted to the Lorentz factor variates as follows,

$$\gamma_{A,n} = 1 + \frac{\gamma_D T_{\perp}}{mc^2} \mathcal{E}_n. \quad (\text{C.2})$$

Then, the random variates of momentum vector are obtained as follows,

$$u_{x,n} = \gamma_D \sqrt{\frac{T_{\parallel}}{T_{\perp}}} \left(c \sqrt{\gamma_{A,n}^2 - 1} \cos \theta_n + \gamma_A v_D \right), \quad (\text{C.3a})$$

$$u_{y,n} = c \sqrt{\gamma_{A,n}^2 - 1} \sin \theta_n \cos \phi_n, \quad (\text{C.3b})$$

$$u_{z,n} = c \sqrt{\gamma_{A,n}^2 - 1} \sin \theta_n \sin \phi_n, \quad (\text{C.3c})$$

where θ_n and ϕ_n are given by using Eq. (24b,c) and Eq. (23) by replacing γ_B with γ_A .

Appendix D. Loading of Non-relativistic Maxwellian Distribution

Random of energy variates from Maxwellian energy distribution are generated by using Eq. (20). The energy variates are converted to scalar velocity variates as follows,

$$v_n = \sqrt{\frac{2T}{m}} \mathcal{E}_n. \quad (\text{D.1})$$

Then, the random variates of velocity vector are obtained as follows,

$$v_{x,n} = v_n \cos \theta_n + v_D, \quad (\text{D.2a})$$

$$v_{y,n} = v_n \sin \theta_n \cos \phi_n, \quad (\text{D.2b})$$

$$v_{z,n} = v_n \sin \theta_n \sin \phi_n, \quad (\text{D.2c})$$

where θ_n and ϕ_n are given by using Eq. (21).

Code availability

A sample code for generating a relativistic shifted-Maxwellian energy distribution in MATLAB [17] is available from <https://github.com/taka-umeda/rela.maxwellian>.

Declaration of generative AI and AI-assisted technologies in the writing process

During the preparation of the final manuscript, the author used Google Gemini for spelling and grammar corrections. After using this tool, the author reviewed and edited the content as needed and take full responsibility for the content of the publication.

Acknowledgment

This work was supported by MEXT/JSPS under Grant-in-Aid (KAKENHI) for Scientific Research (B) No.JP24K00603. A part of numerical calculations were performed on the Interdisciplinary Large-scale Computing System at Information Initiative Center, Hokkaido University. This work was also conducted under joint research programs at Institute for Space-Earth Environmental Research, Nagoya University.

References

- [1] G. E. P. Box and M. E. Muller, A note on the generation of random normal deviates, *Ann. Math. Stat.* 29 (1958) 610–611; <http://dx.doi.org/10.1214/aoms/1177706645>.

- [2] F. Jüttner, Das Maxwellsche Gesetz der Geschwindigkeitsverteilung in der Relativtheorie, *Ann. Phys.* 339 (1911) 856–882; <https://doi.org/10.1002/andp.19113390503>.
- [3] S. Zenitani and S. Nakano, Loading a relativistic Kappa distributions in particle simulations, *Phys. Plasmas* 29 (2022) 113904; <https://doi.org/10.1063/5.0117628>.
- [4] L. A. Pozdnyakov, I. M. Sobol, and R. A. Sunyaev, Comptonization and the shaping of x-ray source spectra-Monte Carlo calculations, *Soviet Sci. Rev. Sec. E: Astrophys. Space Phys. Rev.* 2 (1983) 189–331.
- [5] E. Canfield, W. M. Howard, and E. P. Liang, Inverse comptonization by onedimensional relativistic electrons, *Astrophys. J.* 323 (1987) 565–574; <https://doi.org/10.1086/165853>.
- [6] J. D. Schnittman and J. H. Krolik, A Monte Carlo code for relativistic radiation transport around Kerr black holes, *Astrophys. J.* 777 (2013) 11; <https://doi.org/10.1088/0004-637X/777/1/11>.
- [7] M. Swisdak, The generation of random variates from a relativistic Maxwellian distribution, *Phys. Plasmas* 20 (2013) 062110; <https://doi.org/10.1063/1.4812459>.
- [8] S. Zenitani, Loading relativistic Maxwell distributions in particle simulations, *Phy. Plasmas* 22 (2015) 042116; <https://doi.org/10.1063/1.4919383>.

- [9] S. Zenitani, Modifications to Swisdak (2013)'s rejection sampling algorithm for a Maxwell-Jüttner distribution in particle simulations, *Phys. Plasmas* 31 (2024) 094501; <https://doi.org/10.1063/5.0226859>.
- [10] M. Melzani, C. Winisdoerffer, R. Walder, D. Folini, J. M. Favre, S. Krastanov, and P. Messmer, Apar-T: Code, validation, and physical interpretation of particle-in-cell results, *Astron. Astrophys.* 558 (2013) A133; <http://doi.org/10.1051/0004-6361/201321557>.
- [11] Wolfram Research Inc., *Mathematica* version 14.2, Champaign, IL (2024); <https://www.wolfram.com/mathematica/>.
- [12] G. Livadiotis, Modeling anisotropic Maxwell-Jüttner distributions: derivation and properties, *Ann. Geophys.* 34 (2016) 1145–1158; <http://doi.org/10.5194/angeo-34-1145-2016>.
- [13] A. Soranzo and E. Epure, Very simply explicitly invertible approximations of standard normal cumulative and standard normal quantile function, *Appl. Math. Sci.* 8 (2014) 4323–4341; <https://doi.org/10.12988/ams.2014.45338>.
- [14] T. Umeda, Generation of normal distributions revisited, *Comput. Stat.* 39 (2024) 3907–3921; <https://doi.org/10.1007/s00180-024-01468-3>.
- [15] R. A. Treumann and W. Baumjohann, Anisotropic Jüttner (relativistic Boltzmann) distribution, *Ann. Geophys.* 34 (2016) 737–738; <https://doi.org/10.5194/angeo-34-737-2016>.

- [16] G. Ueno and S. Zenitani, Relativistic Maxwellian mixture model, Phys. Plasmas 28 (2021) 122106; <https://doi.org/10.1063/5.0059126>.
- [17] The Mathworks Inc., MATLAB version R2023a, Natick, MA (2023); <https://www.mathworks.com/products/matlab.html>.